Dynamic evaluation of two configurations for a hybrid DFIG-based wind turbine integrating battery energy storage system

Raúl Sarrias-Mena, Luis M. Fernández-Ramírez, Carlos Andrés García-Vázquez, Francisco Jurado

Published in:
Wind Energy, vol. 18, nº 9, pp. 1561-1577

DOI (link to publication from Publisher):
https://doi.org/10.1002/we.1776

Publication date:
2014

Document Version:
Accepted version

Citation for published version:
R. Sarrias-Mena, L. M. Fernández-Ramírez, C. A. García-Vázquez, F. Jurado, "Dynamic evaluation of two configurations for a hybrid DFIG-based wind turbine integrating battery energy storage system," *Wind Energy*, vol. 18, nº 9, pp. 1561-1577, 11-Jun-2014. https://doi.org/10.1002/we.1776.

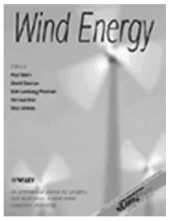

Dynamic evaluation of two configurations for a hybrid DFIG-based wind turbine integrating battery energy storage system

Journal:	*Wind Energy*
Manuscript ID:	WE-13-0013.R1
Wiley - Manuscript type:	Research Article
Date Submitted by the Author:	05-Oct-2013
Complete List of Authors:	Sarrias, Raul; University of Cadiz, Electrical Engineering Fernandez, Luis; University of Cadiz, Electrical Engineering García, Carlos Andrés; UNIVERSITY OF CADIZ, ELECTRICAL ENGINEERING Jurado, Francisco; University of Jaen, Electrical Engineering
Keywords:	Doubly fed induction generator, energy storage system, hybrid system, wind energy

Dynamic evaluation of two configurations for a hybrid DFIG-based wind turbine integrating battery energy storage system

Raúl Sarrias [1], Luis M. Fernández [1,*], Carlos Andrés García [1], Francisco Jurado [2]

[1] *Department of Electrical Engineering, University of Cádiz, 11202 EPS Algeciras, Algeciras (Cádiz), Spain*

[2] *Department of Electrical Engineering, University of Jaén, 23700 EPS Linares, Linares (Jaén), Spain*

Abstract

Hybrid systems comprising batteries energy storage systems (BESSs) and wind power generation entail considerable advances on the grid integration of renewable energy. Doubly-fed induction generators (DFIGs) stand out among different wind turbine (WT) technologies. On the other hand, electrochemical batteries have proved to be valid for these purposes. In this paper, a comparative analysis is carried out between two alternative configurations for hybrid WT-BESS systems, where the BESS is connected either outside or inside the DFIG. The modeling of these two configurations and the control systems applied for achieving the coordinate operation of the energy sources (DFIG and batteries) are illustrated. The hybrid systems under study are evaluated by simulation under normal operation (wind speed fluctuations and grid demand changes) and grid faults. Simulation results show that both configurations improve the grid integration capability of the WT, although the configuration with external BESS presents better results since it can provide additional active/reactive power injection.

[*] Corresponding author. Tel.: +34 956 028166; fax: +34 956 028001.
E-mail addresses: raul.sarrias@uca.es (R. Sarrias), luis.fernandez@uca.es (L. M. Fernández), carlosandres.garcia@uca.es (C. A. García), fjurado@ujaen.es (F. Jurado).

Keywords

Doubly fed induction generator; energy storage system; hybrid system; wind energy.

1. Introduction

Due to the intermittent and uncontrollable nature of wind, large penetration of wind power generation into electric power systems might introduce stability and reliability problems that threaten the proper operation of other suppliers and consumers, especially when connected to weak grids [1]. Problems such as short-term voltage instability, random power fluctuation, lack of energy and voltage management, excessive and uncontrollable reactive power consumption, and defective response to grid faults (e.g. tripping because of overspeed, or slow voltage recovery that may cause tripping of other wind turbines nearby), can be more pronounced when traditional fixed-speed induction generators are used [2-7]. On the other hand, large-scale energy storage systems (ESSs) act as energy accumulators which are readily accessible either to absorb or provide considerable amounts of energy, and thus, being suitable for coupled operation with intermittent renewable energy generators, such as wind power [8]. Therefore, hybrid systems consisting on ESS and wind power present all the main benefits of a sustainable resource, while the ESSs reduce some of the inherent drawbacks of these types of energy supply [9,10].

Currently, two WT technologies dominate the market: DFIG and permanent magnet synchronous generator (PMSG), both based on variable-speed WT. The use of a partial-scale power converter in the former, opposite to a total-scale in the latter, stands out as one

of the main advantages of DFIGs [11-14].

Many different storage devices are commercially available nowadays which are regarded as an adequate back-up system in distributed generation schemes. In this paper, a suitable storage system has been considered for hybrid applications with wind power generators. Ultracapacitors for instance, are seen as effective devices for mitigating short-term wind power fluctuations. They are able to provide a boost of power during short periods, usually in the range of a few seconds or minutes [15,16]. This technology can operate either as a part of an external FACTS (Flexible AC Transmission System) device such as STATCOMs (Static Synchronous Compensator), or as a proper ESS coupled to a WT [7,17-21]. Nonetheless, ultracapacitors are not adequate for the hybrid systems proposed herein, since a longer duration ESS is preferred. This performance can be achieved with hydrogen-based systems comprising electrolyzer, storage tanks and fuel-cells [22]. However, the hydrogen is not yet a cost-competitive technology compared to other ESS [16,23,24]. Electrochemical batteries meet some of the desired characteristics for an ESS in hybrid systems. They show a relatively short time response, while they are able to provide electricity in the range of seconds to a few hours. In particular, lead-acid electrochemical batteries stand out for their maturity, which leads to lower capital costs, and acceptable electric efficiency [15,23]. For these reasons, the lead-acid technology has been chosen as storage device, thus comprising the BESS of the hybrid systems presented in this paper.

Several configurations and control schemes for hybrid systems equipped with batteries and wind power have been proposed in the literature. One of the eligible alternatives is the

aggregated concept, in which a single ESS serves a group of wind generators operating together. Nonetheless, the aim of this paper is to study the performance of a hybrid WT-BESS system which can be connected and operate independently in any point of the grid, not exclusively as a part of a wind farm. Such distributed configuration can be placed at weak nodes of the grid in order to improve reliability and stability of the system. Likewise, it can also be integrated in a wind farm to develop large-scale load leveling.

A feasible solution in distributed generation schemes is to place the BESS outside the generator or wind farm [25,26], which is valid regardless of the WT technology employed. On the other hand, when DFIG-based WT are considered, the DC bus of the DFIG offers an alternative possibility where the BESS can be connected and controlled in coordination with the WT in the hybrid system [27,28]. So far, no relevant study has been carried out where both alternatives are compared under the same operating conditions. Therefore, a comparative analysis of two different configurations of WT-BESS hybrid systems is developed herein.

2. Hybrid Configuration Schemes

Two alternative configurations for the WT-BESS hybrid systems are proposed and compared in this paper, which differ basically in their structure. One of the implemented schemes makes use of the internal structure of the DFIG in order to exchange active power between the BESS and the rest of the system; whereas the other presents an external connection of the BESS to the WT output terminals. Moreover, a base case consisting of a single DFIG driven WT (without any BESS) is also considered in Section 6 to emphasize

the improvements accomplished with the inclusion of a coupled BESS.

2.1. Internal BESS Hybrid System

Regarding the internal structure of the DFIG, it can be clearly seen that the AC/DC/AC power converter allows interconnection of the BESS by using a bidirectional DC/DC converter, as shown in Fig. 1.

Fig. 1. Internal BESS hybrid system configuration

In this configuration, the active power exchanged with the BESS flows through the DFIG grid side converter (GSC). Subsequently, the design parameters of this converter affect the operational boundaries of the BESS. It would be possible to increase the rated power of the GSC in order to allow a higher active power exchange with the BESS. Nonetheless, this option is not considered in this paper, since identical characteristics of the DFIG components are mandatory for the sake of adequate comparison between the internal and external configuration, where oversizing the GSC is not justified.

2.2. External BESS Hybrid System

An alternative configuration can be obtained when the BESS is connected to the WT output terminals. This structure requires additional power converters in order to regulate the power exchange between the components of the hybrid system. Thus, an AC/DC and a DC/DC bidirectional power converter become necessary to adapt the DC battery output to

the grid AC signal.

Fig. 2. External BESS hybrid system configuration

The scheme shown in Fig. 2 avoids the additional power exchange through the GSC observed in the internal BESS configuration, since this transference is now carried out through the external AC/DC converter, which can be sized independently to the DFIG characteristics. Therefore, it is the rated power of this external converter that sets the limitation on the power exchange with the BESS, and this parameter can be chosen conveniently during the design process. Nonetheless, the maximum allowable current of the AC/DC converter has been set to the same value as for the GSC, in order to compare both configurations under the same restrictions during the simulations.

3. Modeling of the Hybrid Systems Components

The main components of the hybrid systems have been modeled using MATLAB/Simulink software. The descriptions presented herein are also applicable to the base case, DFIG without BESS.

3.1. Wind Turbine Mechanical and Electrical Systems

A General Electric Inc. WT equipped with DFIG has been considered [29]. This model is based on the 1.5 MW WT model available in the SimPowerSystems® library [30]. In this model, the mechanical torque generated by the WT rotor is obtained by the actuator disk

theory [31]. According to this theory, the aerodynamic power available in the airstream facing the turbine, P_a, is directly proportional to the swept area of the rotor (A_r), the air density (ρ), and the incoming wind speed (u), as given in Eq. (1).

$$P_a = \frac{1}{2} \cdot A_r \cdot \rho \cdot u^3 \tag{1}$$

Nonetheless, the turbine power capture (P_{wt}) is limited by the power coefficient (C_p) of the WT, which is usually provided by the manufacturer as a function of the tip speed ratio (λ) and the pitch angle of the blades (θ). Hence, the actual power capture of the turbine is given by Eq. (2). Finally, the turbine mechanical torque (T_{wt}) can be obtained with the ratio between the power captured by the blades and the angular speed of the wind turbine (ω_{wt}), as expressed in Eq. (3).

$$P_{wt} = P_a \cdot C_p(\lambda,\theta) = \frac{1}{2} \cdot A_r \cdot \rho \cdot C_p(\lambda,\theta) \cdot u^3 \tag{2}$$

$$T_{wt} = \frac{P_{wt}}{\omega_{wt}} \tag{3}$$

Once T_{wt} is calculated, it serves as an input to the drive train model. The drive train is represented by the two-mass model [32] in order to calculate the mechanical torque (T_m) inputted to the DFIG rotor. In Fig. 3 a block diagram of the rotor and drive train models, and their interaction with the DFIG, is shown. All the representative parameters are illustrated, where R stands for the radius of the wind turbine rotor, ω_r and $\omega_{r\,ref}$ are the generator angular speed and its reference respectively.

Fig. 3. Block diagram of wind turbine and drive train models

A fifth-order model is used for the DFIG [33]. The power converter of the DFIG, which is composed of two back-to-back IGBT bridges (named Rotor Side Converter (RSC) and GSC according to their position) linked by a DC bus, is modeled as an AC/DC/AC PWM converter based on IGBT switches. Proper control of this converter is a crucial factor for the operation of the DFIG, and thus of the hybrid systems, within a desired performance.

3.2. Electrochemical Battery

The electrochemical battery block available in the SimPowerSystems® [30] library has been used in the hybrid systems presented here. This model consists of a variable DC voltage source in series with a resistor that models internal power losses in the device. The design parameters for the electrochemical battery model have been obtained from the Discover Energy Corp. D23000 VRLA cell datasheet [34]. By connecting several cells in series and in parallel, a 750V, 330kW battery has been accomplished. In order to validate the electrochemical battery model, Fig. 4 shows a comparison between the constant current discharge curve obtained from the D23000 device datasheet, and the response provided by the model. As can be seen, both curves match acceptably.

Fig. 4. Discharge curves comparison: D23000 vs. Model

3.3. BESS - DC/DC Converter

Either in the internal or external BESS hybrid system configuration, a DC/DC power converter allows the bidirectional power flow for the charge/discharge of the battery. Its structure consists of two electronic switches based on IGBTs and diodes. Besides, a high frequency inductance filters the input current, whereas a filtering capacitor is located at the output to improve voltage response of the device.

In the hybrid configurations proposed, the DC/DC converter is mainly controlled to regulate the active power exchange with the BESS, as will be described below.

4. Control Schemes for the Hybrid Systems

In this section, the main control schemes implemented in the components of the hybrid systems and the DFIG without BESS are detailed. With the purpose of achieving sufficient homogeneity in the study of both hybrid configurations, the same control schemes have been applied to corresponding elements in the internal and external BESS models.

4.1. DFIG – Rotor Side Converter Controller

A vector control strategy is implemented in the RSC that allows the decoupled control of the active and reactive power generated in the DFIG by acting on the *d* and *q* components of the rotor voltage, respectively, as shown in Fig. 5.

Fig. 5. RSC control scheme

By acting on the *d* component of the rotor voltage, the RSC regulates the total active power generated in the DFIG (P_g), which is the sum of the stator and rotor windings output. The RSC active power control strategy implements a selector that provides two operating modes [35], i.e. *power optimization/limitation*, and *power reduction* mode. The supervisory control system (SCS) generates the switching signal *power reduction* that drives the RSC mode selector depending on the instantaneous operating conditions of the DFIG and BESS. In the *power optimization/limitation* mode, the DFIG active power-speed curve is used to define the active power reference in the RSC controller according to the actual generator speed.

On the other hand, in the *power reduction* mode, the SCS directly determines the RSC active power reference. This operating mode is based on the coupled operation of the electrical and mechanical systems of the WT. Since the new reference is lower than the optimal value, the whole system must be able to reduce the overall power exchange. This curtailment is accomplished by means of the RSC and the pitch controller operating coordinately. Hence, as the RSC reaches a lower active power generation through the PI-based control loops implemented (fast electrical response), the wind turbine angular speed accelerates because of the input/output power imbalance. Consequently, the pitch angle increases to reduce the aerodynamic power capture (slow mechanical response), thus recovering the stable operation in a new active power generation value.

The RSC controller also regulates the reactive power generation by acting on the *q*

component of the rotor voltage. The total reactive power generation in DFIGs corresponds to the sum of the reactive power provided by the stator windings, Q_s, and the fraction supplied through the GSC, Q_{gsc}. Here, only Q_s is considered, since Q_{gsc} is controlled on the GSC and will be described later on. The stator reactive power reference, Q_s^*, is set by the SCS according to a hierarchical distribution of the grid demand.

4.2. DFIG – Grid Side Converter Controller

Decoupled vector control has also been implemented in the GSC. This controller is responsible for maintaining the DFIG DC bus voltage close to its reference, and regulating the reactive power flow through the GSC independently. Similarly to the RSC, this can be accomplished by acting on the *d* and *q* components of the AC voltage at the grid side of the converter, respectively. The control scheme implemented for the GSC is shown in Fig. 6.

In this case, the control of the DC bus voltage is performed by acting on the *d* component of the grid side voltage. On the other hand, the *q* component of the grid side voltage is used to regulate the reactive power flow through the GSC. Similarly to the RSC, the reactive power reference for the GSC, Q_{gsc}^*, is set by the hierarchical strategy implemented in the SCS.

Fig. 6. GSC control scheme

In Figs. 5 and 6, compensation terms have been added to u_{dqr}^* and u_{dqg}^* control loops respectively. These terms, which are derived from the equations of rotor voltage

(compensation terms added to u_{dqr}^{*}) and grid side voltage (compensation terms added to u_{dqg}^{*}), allow obtaining a linear transfer function between the currents and the controller output voltages [36,37].

4.3. BESS – DC/DC Converter Controller

Fig. 7 shows the control scheme adopted to drive the switching cycles of the IGBT-diodes switches that comprise the DC/DC converter. The designed control system allows two different operating modes, which are automatically selected depending on the operation of the hybrid systems.

Fig. 7. DC/DC converter control scheme

The *normal operation* mode is defined as the state when no grid voltage contingencies appear. Then, the BESS is controlled to follow the active power reference imposed by the SCS. Thus, active power is stored in or released by the battery according to the grid demand and battery SOC. As seen in Fig. 7, this can be achieved with a single PI controller-based control loop to define the duty cycle that drives the IGBT switches.

The *voltage sag operation* mode is activated when the grid voltage drops below a previously defined limit. Under these conditions, it is important to regulate the DC voltage of the bus where the battery is connected, avoiding large fluctuations of the DC voltage that hamper a fast recovery of the hybrid system after clearing the fault. Again, a single control loop based on PI-controller is adequate to generate the duty cycle of the IGBTs.

4.4. BESS – AC/DC Converter Controller

Exclusively in the case when the BESS is connected externally to the DFIG, an AC/DC converter becomes necessary to transform the output of the BESS – DC/DC converter into AC at the grid specific voltage and frequency.

Similarly to the GSC of the DFIG, its main purpose is to allow a bidirectional active and reactive power exchange between a DC bus and the grid. Hence, the AC/DC converter implemented in the external BESS configuration has been modeled as a back-to-back IGBT bridge. In the implemented control strategy, the voltage of the DC bus formed between the DC/DC and the AC/DC converters is controlled by acting on the *d* component of the AC grid side voltage. On the other hand, the reactive power flow through this converter, named here Q_{ess}, is regulated through the *q* component of the same voltage. Therefore, this control strategy shows an identical scheme to that detailed for the GSC of the DFIG.

5. Supervisory Control System (SCS)

Coordinate operation of BESS and DFIG in a hybrid system is achieved by action of the SCS. This system sets the active and reactive power references for the controllers described in the previous section, taking into account different parameters, such as battery SOC and grid demand.

5.1. SCS – Active Power Reference

The SCS is responsible for setting the battery active power reference as a function of its SOC. Besides, it also activates the *power reduction* mode in the RSC when necessary.

A truth table block is used to determine the active power reference in the SCS. This block presents as inputs the active power mismatch (calculated as the difference between the DFIG active power generation and the grid demand), the active power through the rotor windings of the DFIG, and the instantaneous battery SOC. As outputs, the battery active power reference and the *power reduction* switching signal are delivered to their respective controllers.

Seven states are used in the truth table, depending on the value of the defined inputs and internal variables. For every state, the battery active power reference is calculated in a different manner, in order to avoid the battery SOC to exceed the recommended values, i.e. a minimum of 30% and a maximum of 70%. A more detailed explanation on the design and operation of this SCS can be found on [38,39].

5.2. SCS – Reactive Power Reference

A hierarchical control strategy has been chosen to define the reactive power references required for the BESS (through its AC/DC converter when it is located outside the DFIG), the stator windings of the DFIG, and the GSC. This approach defines a ranking, according to which the element of a lower level will not exchange reactive power until the elements

corresponding to the upper levels have reached their limit. Finally, the total sum of the reactive power through all the components must equal the grid demand. In the implemented hierarchical structure, the BESS receives the first request to adapt to grid demand. Nonetheless, as previously indicated, the BESS will only be able to exchange reactive power when it is connected outside the DFIG, since when the BESS appears inside the DFIG, the reactive power flows through the GSC, and therefore it counts as Q_{gsc}. Following the BESS, the stator is the second element to support reactive power generation/consumption when necessary. Finally, the GSC will be controlled to exchange the required reactive power in order to fulfill the grid demand when the upper components reach their maximum current limitation.

6. Simulations Results and Discussion

Three different cases study have been considered in order to compare the performance of the hybrid systems proposed. The base case (denoted as *w/o*, which stands for without BESS, in the following figures) is used as a reference to highlight the improvements achieved with the implementation of BESS in the hybrid schemes.

6.1. Case Study 1: Variable Wind Speed and Grid Demand

In this case study, the ability of the hybrid systems to supply an externally set active and reactive power demand, while operating under wind fluctuations, is analyzed. This is to verify the adequate operation of the control schemes implemented on the DFIG and BESS converters, as well as the SCS. The aim is to achieve a proper adjustment of the hybrid

systems output to variations on the grid power demand, as required by the TSO, providing a controlled power generation similarly to traditional power plants. This performance pursues the reduction of uncertainty, unpredictability and variability of wind power generation with the implementation of a BESS.

During the simulation, the wind fluctuates both above and below the rated value, thus making the WT to operate in the optimization and limitation modes. Hence, the incoming wind speed remains above the WT nominal value during the first 135s, and below this limit up to the end of the simulation.

In addition, active power grid demand varies in three levels, in order to show both charging and discharging operation of the BESS. This demand is set at 1.3pu during the first 80s, then it decreases (with a slew rate of 0.1pu/s) to 0.5pu until 160s, when it increases to the WT rated value, 1pu. Therefore, the grid requirements are independent from the captured DFIG mechanical power, P_m, which is close to 1pu as long as the wind speed remains above its rated value, and fluctuates proportionally to the wind for below rated speeds.

As seen in Fig. 8, the total output active power generated by the external and internal BESS configurations of the hybrid systems (namely *Ext* and *Int* respectively) are quite similar. On the other hand, the response of the model without BESS varies with the wind speed, following the DFIG mechanical power (P_m), without performing any management on the active power output. Hence, the hybrid systems are able to partially decouple, within a certain limits, active power generation from the actual wind conditions.

When, at 160s, the grid demand increases up to 1pu, and the wind speed is low, the BESS must provide a large amount of power in order to address the grid requirements. Hence, the BESS current rises rapidly and reaches its limitation (1500A), as seen in Fig. 9. As a consequence, the BESS is not able to supply all the active power needed to satisfy grid demand, and it is partially unaddressed in some periods between 160s and 240s, when the wind power capture is low.

Moreover, two disturbances appear at 35s and 72s. In Fig. 8, it can be seen that the internal BESS hybrid system deviates notably from the power reference. This deviation is a consequence of large wind speed fluctuations occurred at these instants. Nonetheless, this effect is reduced in the external BESS configuration. This is due to the higher current provided by the external BESS, as seen in Fig. 9, during the disturbances. In the internal BESS configuration, the GSC of the DFIG is close to its current limit previously to the deviations. Hence, when a current boost is necessary, the GSC soon reaches its limits and is not able to fulfill the requirements, and therefore the total output power decreases, deviating from the grid demand. This transitory power drop turns into a gust above the reference as the BESS current recovers more slowly in the internal configuration.

Fig. 8. Active power output (case 1)

Fig. 9. BESS output current (case 1)

Fig. 10. Total reactive power output (case 1)

Fig. 9 also shows the bidirectional power flow in the battery, which can be noticed regarding the sign of the battery current. Hence, for positive values of this current, the battery releases energy to support the WT generation to grid; whereas it is negative during storage periods when the WT active power generation exceeds the grid demand.

A variable grid reactive power demand has also been set for the hybrid systems, which comprises a generation of 1.1pu during the first 120s, and a consumption of 0.2pu from this moment up to the end of the simulation. This ability to supply/absorb reactive power gives the hybrid systems the capacity to regulate voltage.

Fig. 10 shows the total reactive power output of both hybrid system configurations and the model without BESS. It can be clearly seen that the internal BESS structure and the single DFIG are not able to completely address the grid demand when large reactive power generation is required, whereas the external BESS configuration matches adequately the reactive power reference during the whole simulation.

Fig. 11. BESS reactive power output (case 1)

Fig. 12. Stator reactive power output (case 1)

Fig. 13. GSC reactive power output (case 1)

According to the hierarchical structure described, different elements are responsible for

addressing the changes in this reference. Firstly, the external BESS configuration provides a considerable fraction of 0.7pu during the initial interval, and absorbs 0.2pu in the second period, which is the total amount required by the grid (Fig. 11). However, as stated before, in the internal BESS structure, the battery output is transmitted to grid via the GSC. Therefore, no additional BESS reactive power supply is available in the internal BESS or single DFIG configurations. Since the BESS is not able to provide the demanded reactive power completely, the stator must supply the remaining in the three configurations, as seen in Fig. 12.

For the first 120s, the three structures perform similarly, providing the maximum reactive power through the stator windings according to the wind conditions. The external BESS configuration reduces the reactive power generation as soon as the grid demand decreases, and becomes null during the reactive power consumption period. On the other hand, the internal BESS and single DFIG configurations are required to generate reactive power through the stator until 128s, when the grid demand decreases below the maximum stator limit. Then, the stator reactive power output turns to 0.2pu absorption, as demanded by the grid. Finally, the GSC compensates the fraction of reactive power that the previous elements are not able to provide or absorb, as depicted in Fig. 13.

6.2. Case Study 2: Moderate Voltage Sag (0.8pu, 1s)

A second case study has been considered, in which the responses of the hybrid systems to a moderate voltage sag at the PCC (voltage of 0.8pu and duration of 1s) are compared. In this simulation, a constant wind speed of 14m/s is considered as input for the WTs, since

wind speed fluctuations are slower than the electric dynamics studied herein. Besides, a constant active power grid demand of 1pu is applied. On the other hand, the reactive power reference is set to zero during normal operation, whereas when the voltage sags occur, all the systems are required to follow the V_{PCC} vs. $I_{reactive}/I_{rated}$ curve presented in [40]; where V_{PCC} is voltage at the PCC, $I_{reactive}$ is the reactive component of the output current, and I_{rated} is the rated current of the WT.

Fig. 14 shows the total active power of the hybrid systems and the DFIG without BESS. Systems initiate the simulation in normal operation providing 1pu of active power to grid. As the voltage sag occurs at 1s, the power supply drops to 0.7pu in the three configurations. Nonetheless, in the external BESS structure, the output active power increases notably during the fault, and approaches its reference of 1pu by the end of the voltage sag; whereas the internal BESS and the single DFIG stabilize approximately at 0.86 and 0.85pu respectively, remaining lower than the external BESS supply during the perturbation. After the fault is cleared at 2s, the three systems recover their reference shortly.

Fig. 14. Total active power output (case 2)

As seen in Fig. 15, both hybrid configurations perform similarly under normal operation. A higher battery output power is achieved for the external BESS configuration during the fault. At the end of the voltage sag, the battery releases 0.17pu to the grid in the external structure, whereas the internal reaches a value close to 0.035pu. This difference eventually becomes certainly significant regarding the total output active power.

The total reactive power output is represented in Fig. 16. No remarkable differences appear between the configurations, since they follow the reference adequately. In all cases, a constant reactive power generation of 0.08pu is achieved after the first 0.2s from the detection of the fault, which helps supporting the voltage recovery.

Fig. 15. BESS active power output (case 2)

Fig. 16. Total reactive power output (case 2)

6.3. Case Study 3: Intense Voltage Sag (0.2pu, 0.5s)

A more demanding voltage sag has also been simulated. The drop is 80% of the nominal value, reaching a voltage of 0.2pu at PCC during 0.5s. It corresponds to the lowest limit that Spanish wind farms must be able to ride through [40].

A constant wind speed of 8m/s, and a constant active power grid demand of 0.6pu have been considered. This grid demand corresponds to a value higher than the wind power capture for the wind speed indicated. Hence, the batteries are required to provide energy during normal operation in this simulation.

As seen in Fig. 17, the hybrid systems properly address the grid demand before and after the fault. On the contrary, these requirements cannot be satisfied by the single DFIG without BESS. Moreover, during the voltage sag, the active power generation drops

drastically for the three configurations considered. Opposite to the previous case, here the internal BESS configuration reaches a higher active power generation during the voltage sag, since a value of 0.31pu is registered, whereas 0.21pu is measured for the external arrangement. This is a consequence of the WT operating regime. With an incoming wind speed of 8m/s, the DFIG runs in the sub-synchronous region. Hence, it consumes active power through the rotor windings. This consumption is compensated with the battery in the internal BESS connection. However, it is subtracted to the total DFIG generation in the external BESS configuration.

Fig. 17. Total active power output (case 3)

Fig. 18. BESS active power output (case 3)

Fig. 19. Total reactive power output (case 3)

Fig. 20. Voltage at the DFIG stator windings (case 3)

During the voltage sag, the GSC output power drops, and this effect becomes more critical for the external BESS. Besides, the battery active power injection (Fig. 18) is also higher for the internal BESS during the perturbation. This contributes significantly to the differences observed in the active power.

Remarkable differences are also observed in the total reactive power, shown in Fig. 19. During the voltage sag, the external BESS configuration injects a total of 0.71pu of reactive

power to grid, whereas the internal supplies 0.48pu as maximum shortly after the fault detection, decreasing to 0.41pu by the end of the perturbation. In the case of the DFIG without BESS, the total reactive power output remains at 0.41pu throughout the voltage sag. On the other hand, the three systems accomplish their reference of zero reactive power before and after the fault occurrence. Basically, this dissimilar performance between the hybrid schemes is a consequence of the additional reactive power provided by the BESS in the external configuration. This extra injection is not available when the battery is connected to the DC bus of the DFIG, since the reactive power flow is controlled in the GSC in this case. Hence, when the battery is located outside the generator, a supplementary reactive power exchange appears, that improves the performance of the external BESS hybrid system both under normal and fault operation.

Finally, the benefits of a superior reactive power injection during voltage sags can be observed in Fig. 20. Regarding the stator voltage, it can be seen that the external BESS configuration achieves a higher voltage during the voltage sag, compared to the response of the internal BESS and single DFIG structures, due to the increased reactive power generation registered. Moreover, all the systems recover their normal operation within 0.2s after the fault clearance, showing an adequate response under demanding grid disturbance conditions.

7. Conclusions

Two WT-BESS hybrid system configurations have been presented and compared in this paper. Modeling and control of DFIG, battery and power converters have been

described. Three case study simulations have been carried out in order to depict the behavior of the most relevant variables.

Dynamic response of the hybrid systems has proved to be adequate under the simulation conditions imposed. Both configurations have been able to satisfactorily address active and reactive power grid requirements when subjected to variable incoming wind speed in almost all cases. Nonetheless, two main limitations appeared, such as the maximum allowable battery current, and maximum reactive power generation in the internal BESS. Hence, there exist certain bounds to the exploitation of the hybrid systems. If they are not exceeded, the inclusion of a BESS improves the performance of wind turbines, and allows decoupling the generation from the wind conditions, thus adapting to grid demand variations.

In addition, hybrid systems have been able to ride through voltage sags at the PCC, showing an adequate response during the fault, and recovering shortly to the steady-state operation after the fault clearance. As previously stated, the external BESS configuration bears an additional active and reactive power support due to the AC/DC converter set for the external connection of the battery. This expands the hybrid system generation boundaries compared to the internal BESS alternative. Hence, an extra power injection can be achieved in certain situations. The expanded generation boundaries of the external BESS configuration contribute significantly to improve the performance of the hybrid system.

Acknowledgements

This work was supported in part by the University of Cádiz under the Grant FPI 2012-036, by the Spanish Ministry of Science and Innovation under Grant ENE2010-19744/ALT, and by the Foundation Technological Campus of Algeciras.

Appendix: Nomenclature

Acronyms

BESS – Battery energy storage system.

DFIG – Doubly-fed induction generator.

ESS – Energy storage system.

FACTS – Flexible AC transmission system.

GSC – DFIG grid side converter.

PCC – Point of common coupling.

PMSG – Permanent magnet synchronous generator.

RSC – DFIG rotor side converter.

SCS – Supervisory control system.

SOC – State-of-charge of the energy storage system.

STATCOM – Static synchronous compensator.

VRLA – Valve-regulated lead-acid.

WT – Wind turbine.

Parameters

A_r – Swept area of the wind turbine rotor.

C_p – Power coefficient of the wind turbine.

d_c (*) – DC/DC converter duty cycle (reference).

i_{dqg}, i_{dqr}, i_{dqs} (*) – Direct and quadrature components of the GSC, rotor and stator currents

(references).

$I_{reactive}$ – Reactive component of the hybrid system output current.

I_{rated} – Rated current of the wind turbine.

L_{lr}, R_r – Rotor windings electrical inductance and resistance.

L_m – DFIG mutual inductance.

L_{RL}, R_{RL} – GSC output filter electrical inductance and resistance.

P_a – Aerodynamic power in the airstream facing the turbine.

P_{ess}, Q_{ess} (*) – Active and reactive power through the ESS (reference).

P_g (*) – Total (sum of stator and rotor) DFIG active power generation (reference).

P_{gsc}, Q_{gsc} (*) – Active and reactive power through the GSC of the DFIG (reference).

P_m – DFIG mechanical power.

P_r, Q_r – Active and reactive power through the rotor windings of the DFIG.

P_s, Q_s (*) – Active and reactive power through the stator windings of the DFIG (reference).

P_t, Q_t – Total active and reactive power output of the hybrid systems.

P_{wt} – Wind turbine mechanical power.

R – Radius of the wind turbine rotor.

T_m – Drive train mechanical torque.

T_{wt} – Wind turbine mechanical torque.

u – Wind speed.

$u_{dqg}{}^*$, $u_{dqr}{}^*$ – Compensated direct and quadrature components of the GSC and rotor voltages.

$u_{dqg}{}'$, $u_{dqr}{}'$ – Direct and quadrature components of the GSC and rotor voltages before compensation.

u_{dqs} – Direct and quadrature components of the stator voltage.

$u_{g\,abc}$, $u_{r\,abc}$ – Three-phase GSC and rotor voltages.

$V_{dc}\,(^{*})$ – DC-bus voltage (reference).

V_{PCC} – Voltage at the point of common coupling.

Greek

θ – Blades pitch angle.

λ – Tip speed ratio.

ρ – Air density.

ω – DFIG synchronous speed.

ω_r – DFIG angular speed.

$\omega_{r\,ref}$ – DFIG angular speed reference.

ω_{wt} – Wind turbine angular speed.

References

[1] Gjengedal T. Large-scale wind power farms as power plants. *Wind Energy* 2005;**8(3)**:361-373. DOI:10.1002/we.165

[2] Akhmatov V, Knudsen H. Large penetration of wind and dispersed generation into Danish power grid. *Electric Power Systems Research* 2007;**77**:1228-1238. DOI:10.1016/j.epsr.2006.08.009

[3] Lund H. Large-scale integration of wind power into different energy systems. *Energy* 2005;**30**:2402-2412. DOI:10.1016/j.energy.2004.11.001

[4] Gautam D, Vittal V, Harbour T. Impact of increased penetration of DFIG-based wind turbine generators on transient and small signal stability of power systems. *IEEE*

Transactions on Power Systems 2009;**24(3)**:1426-1434. DOI:10.1109/TPWRS.2009.2021234

[5] Shi L, Xu Z, Hao J, Ni Y. Modelling analysis of transient stability simulation with high penetration of grid-connected wind farms of DFIG type. *Wind Energy* 2007;**10**:303-320. DOI:10.1002/we.223

[6] Rodríguez JM, Fernández JL, Beato D, Iturbe R, Usaola J, Ledesma P, Wilhelmi JR. Incidence on power system dynamics of high penetration of fixed speed and doubly fed wind energy systems: Study of the Spanish case. *IEEE Transactions on Power Systems* 2002;**17(4)**:1089-1095. DOI:10.1109/TPWRS.2002.804971

[7] Muyeen SM, Shishido S, Ali MH, Takahashi R, Murata T, Tamura J. Application of energy capacitor system to wind power generation. *Wind Energy* 2008;**11**:335-350. DOI:10.1002/we.265

[8] Bousseau P, Fesquet F, Belhomme R, Nguefeu S, Thai TC. Solutions for the grid integration of wind farms –A survey. *Wind Energy* 2006;**9**:13-25. DOI:10.1002/we.177

[9] Kear G, Shah AA, Walsh FC. Development of the all-vanadium redox flow battery for energy storage: a review of technological, financial and policy aspects. *International Journal of Energy Research* 2012;**36**:1105-1120. DOI:10.1002/er.1863

[10] Paatero JV, Lund PD. Effect of energy storage on variations in wind power. *Wind Energy* 2005;**8**:421-441. DOI:10.1002/we.151

[11] Fernández LM, García CA, Saenz JR, Jurado F. Equivalent models of wind farms by using aggregated wind turbines and equivalent winds. *Energy Conversion and Management* 2009;**50(3)**:691-704. DOI:10.1016/j.enconman.2008.10.005

[12] Hansen AD, Hansen LH. Wind turbine concept market penetration over 10 years (1995-2004). *Wind Energy* 2007;**10(1)**:81-97. DOI:10.1002/we.210

[13] Vinothkumar K, Selvan MP. Novel scheme for enhancement of fault ride-through capability of doubly fed induction generator based wind farms. *Energy Conversion and Management* 2011;**52(7)**:2651-2658. DOI:10.1016/j.enconman.2011.01.003

[14] Li H, Chen Z. Overview of different wind generator systems and their comparisons. *IET Renewable Power Generation* 2008;**2(2)**:123-138. DOI:10.1049/iet-rpg:20070044

[15] Hadjipaschalis I, Poullikkas A, Efthimiou V. Overview of current and future energy storage technologies for electric power applications. *Renewable and Sustainable Energy Reviews* 2009;**13(6-7)**:1513-1522. DOI:10.1016/j.rser.2008.09.028

[16] Ibrahim H, Illinca A, Perron J. Energy storage systems –Characteristics and comparisons. *Renewable and Sustainable Energy Reviews* 2008;**12(5)**:1221-1250. DOI:10.1016/j.rser.2007.01.023

[17] Hossain MJ, Pota HR, Ugrinovskii V, Ramos RA. Decentralized control to augment LVRT capability of wind generators with STATCOM/ESS. In: *Proceeding of the IEEE Power and Energy Society General Meeting*, July 2010. DOI:10.1109/PES.2010.5590225

[18] Rahim AHMA, Nowicki EP. Supercapacitor energy storage system for fault ride-through of a DFIG wind generation system. *Energy Conversion and Management* 2012;**59**:96-102. DOI:10.1016/j.enconman.2012.03.003

[19] Banos C, Aten M, Cartwright P, Green TC. Benefits and control of STATCOM with energy storage in wind power generation. In: *Proceeding of the IEEE International Conference on AC and DC Power Transmission*, March 2006.

[20] Qu L, Qiao W. Constant power control of DFIG wind turbines with supercapacitor energy storage. *IEEE Transactions on Industry Applications* 2011;**47(1)**:359-367. DOI:10.1109/TIA.2010.2090932

[21] Abbey C, Joos G. Supercapacitor energy storage for wind energy applications. *IEEE Transactions on Industry Applications* 2007;**43(3)**:769-776. DOI:10.1109/TIA.2007.895768

[22] Yang WJ, Aydin O. Wind energy-hydrogen storage hybrid power generation. *International Journal of Energy Research* 2001;**25**:449-463. DOI:10.1002/er.696

[23] Evans A, Strezov V, Evans TJ. Assessment of utility energy storage options for increased renewable energy penetration. *Renewable and Sustainable Energy Reviews* 2012;**16(6)**:4141-4147. DOI:10.1016/j.rser.2012.03.048

[24] Beaudin M, Zareipour H, Schellenberglabe A, Rosehart W. Energy storage for mitigating the variability of renewable electricity sources: An updated review. *Energy for Sustainable Development* 2010;**14(4)**:302-314. DOI:10.1016/j.esd.2010.09.007

[25] Teleke S, Baran ME, Huang AQ, Bhattacharya S, Anderson L. Control strategies for battery energy storage for wind farm dispatching. *IEEE Transactions on Energy Conversion* 2009;**24(3)**:725-732. DOI:10.1109/TEC.2009.2016000

[26] Jenkins DP, Fletcher J, Kane D. Model for evaluating impact of battery storage on microgeneration systems in dwellings. *Energy Conversion and Management* 2008;**49(8)**:2413-2424. DOI:10.1016/j.enconman.2008.01.011

[27] Jiang Z, Yu X. Modeling and control of an integrated wind power generation and energy storage system. In: *Proceeding of the IEEE Power and Energy Society General Meeting*, July 2009. DOI:10.1109/PES.2009.5275753

[28] Jin C, Wang P. Enhancement of low voltage ride-through capability for wind turbine driven DFIG with active crowbar and battery energy storage system. In: *Proceeding of the IEEE Power and Energy Society General Meeting*, July 2010. DOI:10.1109/PES.2010.5588180

[29] GE 1.5MW Series Wind Turbine, General Electric Inc. [Online]. Available: http://www.ge-energy.com/products_and_services/products/wind_turbines/ge_1.5_77_wind_turbine.jsp. [Last accessed: Jun. 2012]

[30] SimPowerSystems™, Hydro-Québec/the MathWorks Inc., Natick, MA, 2010.

[31] Heier S. *Grid Integration of Wind Energy Conversion Systems*. John Wiley and Sons, 1998.

[32] Slootweg JG. *Wind power modelling and impact on power system dynamics*. Ph.D. Thesis, TU Delft University of Technology, Delft, Netherlands, 2003.

[33] Krause PC, Wasynczuk O, Sudhoff SD. *Analysis of Electric Machinery and Drive Systems*. IEEE Press Series on Power Engineering. John Wiley and Sons, 2002.

[34] Datasheet Discover D Series VRLA Industrial Batteries, part no. D23000, Discover Energy Corp. [Online]. Available: http://www.discover-energy.com/files/datasheets/D23000.pdf. [Last accessed: Feb. 2012]

[35] Fernández LM, García CA, Jurado F. Comparative study on the performance of control systems for doubly fed induction generator (DFIG) wind turbines operating with power regulation. *Energy* 2008;**33(9)**:1438-1452. DOI:10.1016/j.energy.2008.05.006

[36] Peña R, Cardenas R, Asher GM, Clare JC, Rodriguez J, Cortes P. Vector control of a diesel-driven doubly fed induction machine for a stand-alone variable speed energy

system. In: *Proceeding of the IEEE 28th Annual Conference of the Industrial Electronics Society*, Nov 2002. DOI:10.1109/IECON.2002.1185406

[37] Peña R, Clare JC, Asher GM. Doubly fed induction generator using back-to-back PWM converters and its application to variable-speed wind-energy generation. *IEE Proceedings – Electric Power Applications* 1996;**143(3)**:231-241. DOI: 10.1049/ip-epa:19960288

[38] Sarrias R, Fernández LM, García CA, Jurado F. Supervisory control system for DFIG wind turbine with energy storage system based on battery. In: *Proceeding of the IEEE International Conference on Power Engineering, Energy and Electrical Drives*, May 2011. DOI:10.1109/PowerEng.2011.6036489

[39] Sarrias R, Fernández LM, García CA, Jurado F. Coordinate operation of power sources in a DFIG wind turbine/battery hybrid power system. *Journal of Power Sources* 2012;**205**:354-366. DOI:10.1016/j.jpowsour.2012.01.005

[40] Requirements of response against voltage sags in wind power generation facilities (P.O. 12.3), Spanish TSO Red Eléctrica de España [Online]. Available: http://www.ree.es/operacion/pdf/po/ PO_resol_12.3_Respuesta_huecos_eolica.pdf. [Last accessed: Jul. 2012].

LIST OF FIGURES

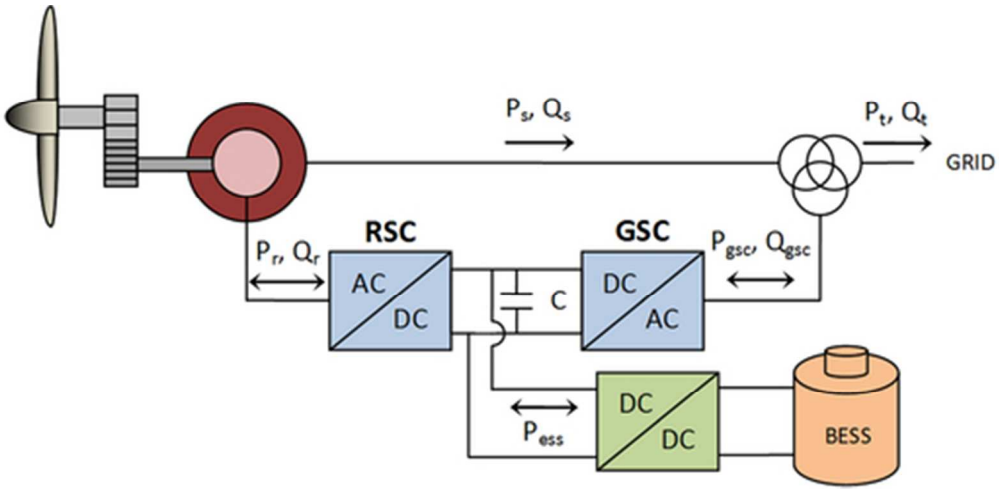

Figure 1
43x20mm (300 x 300 DPI)

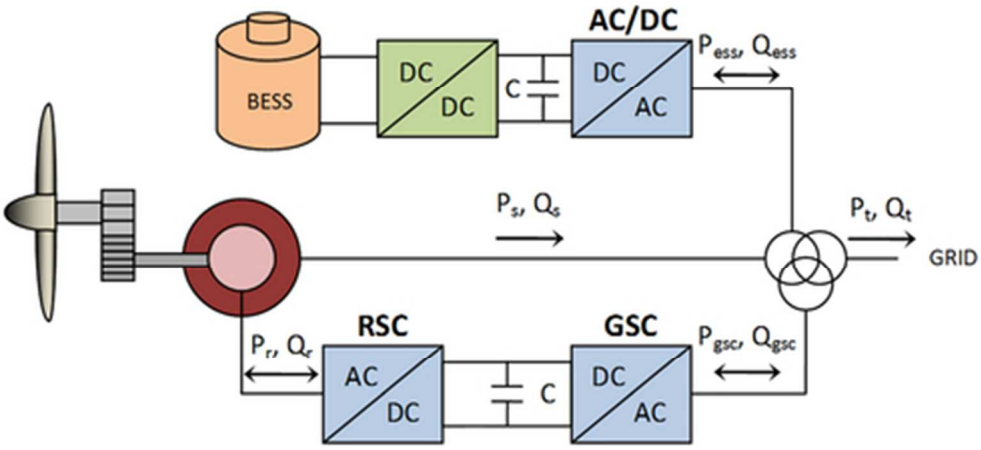

Figure 2
41x19mm (300 x 300 DPI)

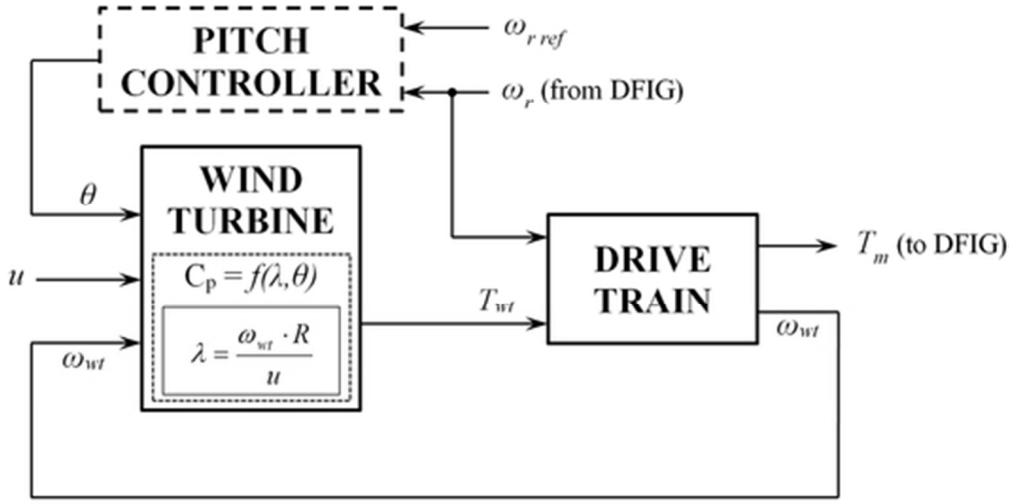

Figure 3
44x22mm (300 x 300 DPI)

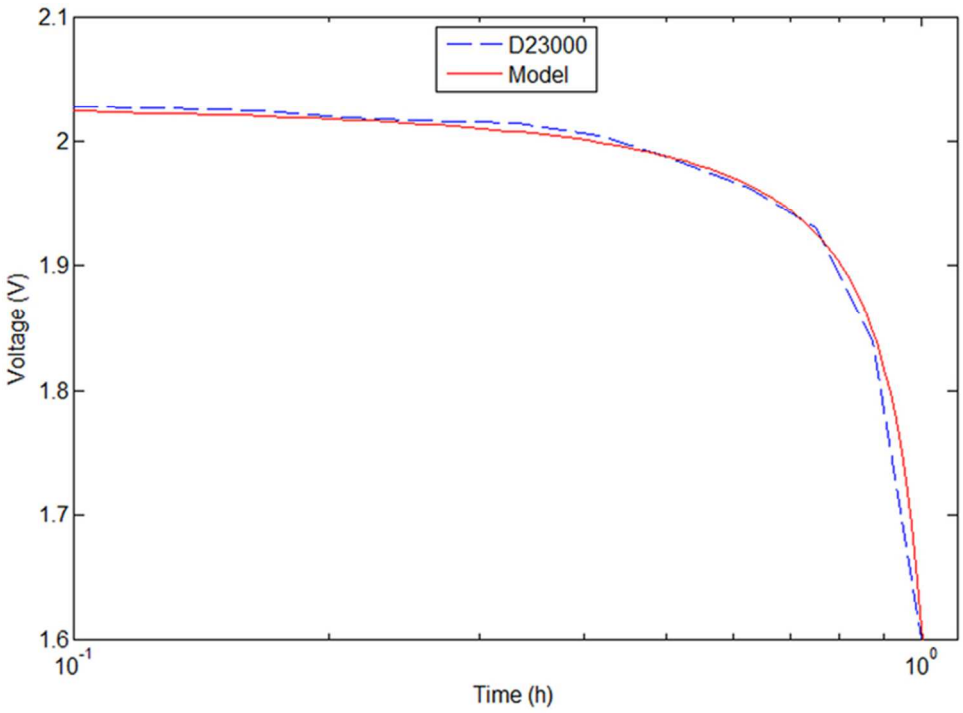

Figure 4
64x46mm (300 x 300 DPI)

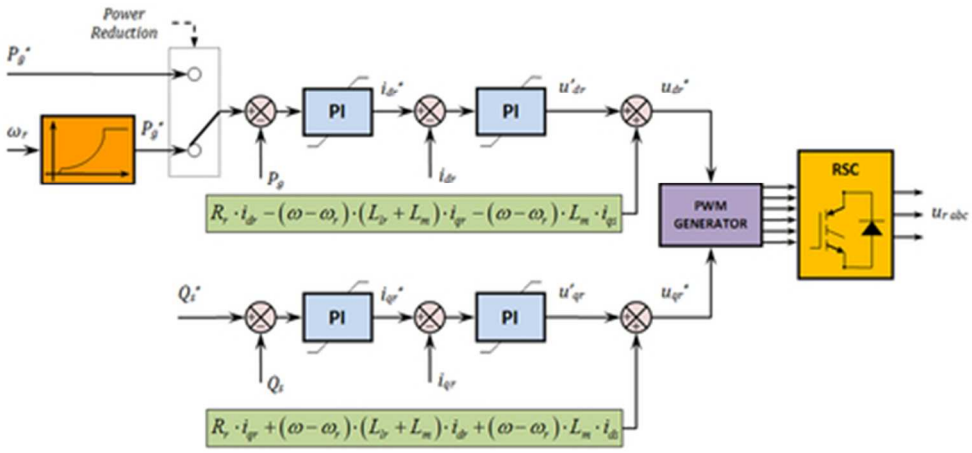

Figure 5
41x18mm (300 x 300 DPI)

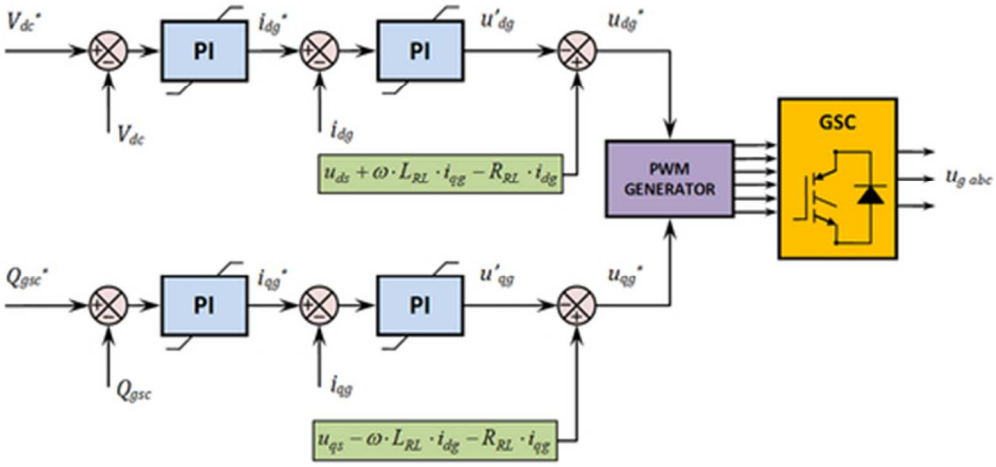

Figure 6
42x20mm (300 x 300 DPI)

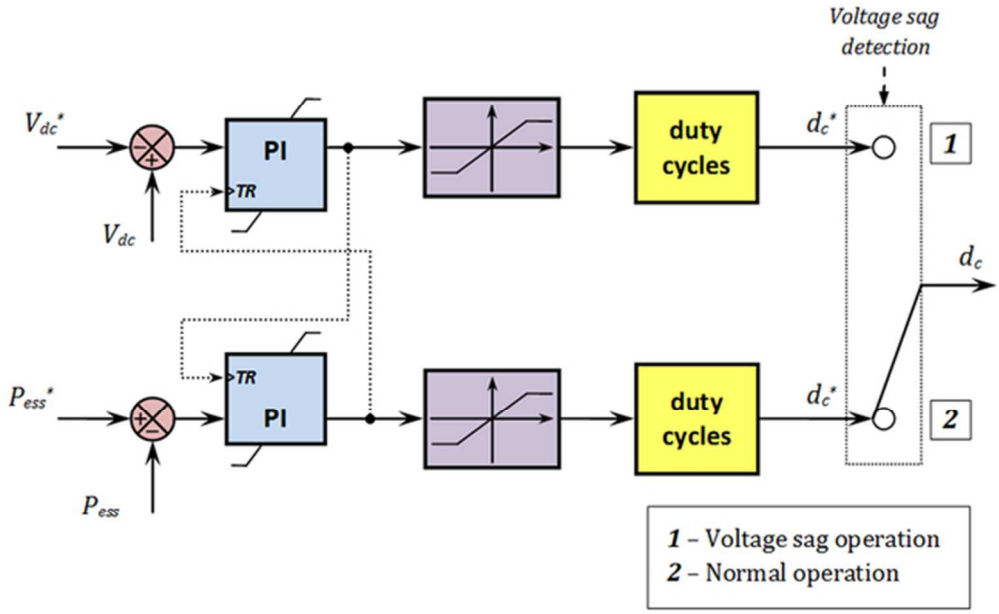

Figure 7
54x33mm (300 x 300 DPI)

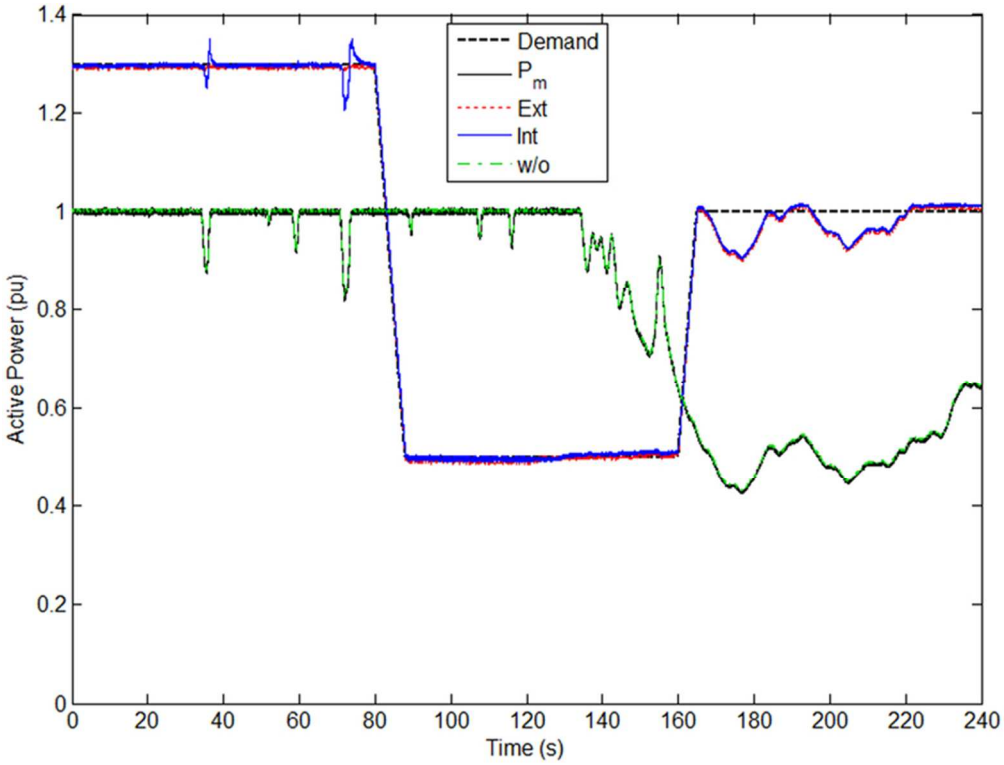

Figure 8
68x51mm (300 x 300 DPI)

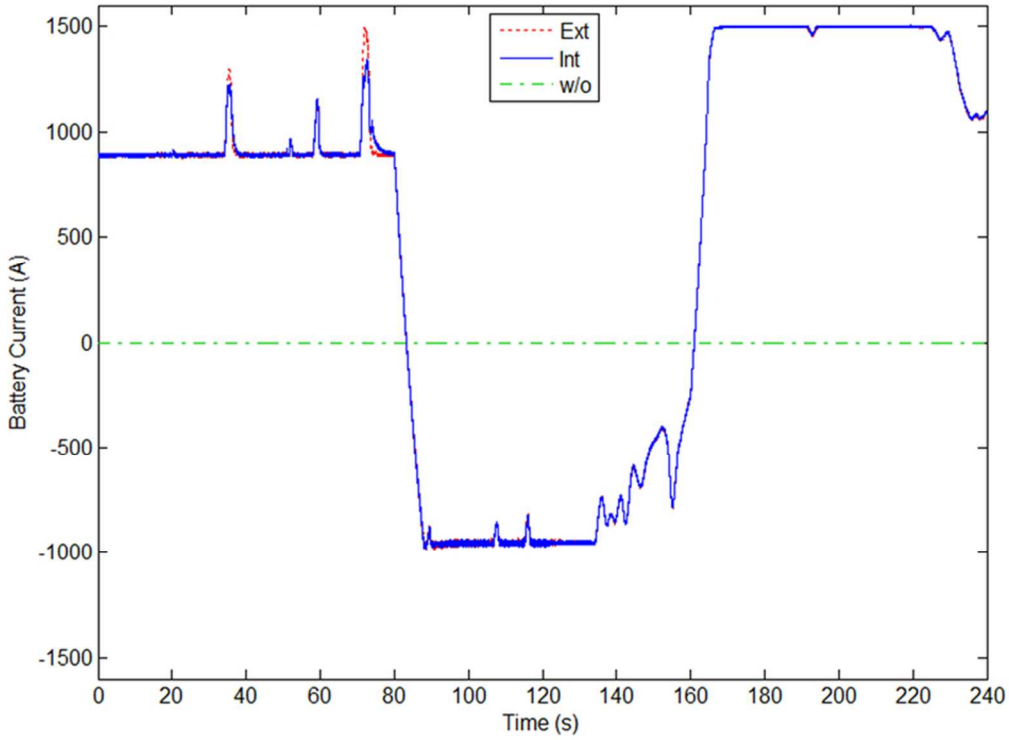

Figure 9
68x52mm (300 x 300 DPI)

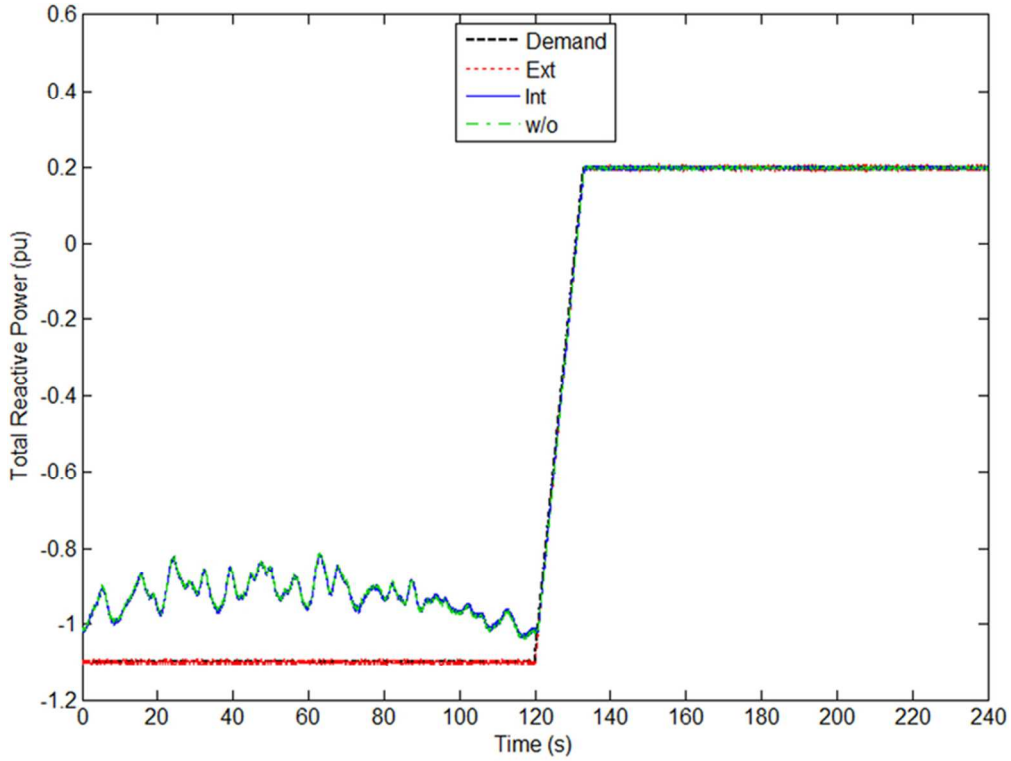

Figure 10
68x51mm (300 x 300 DPI)

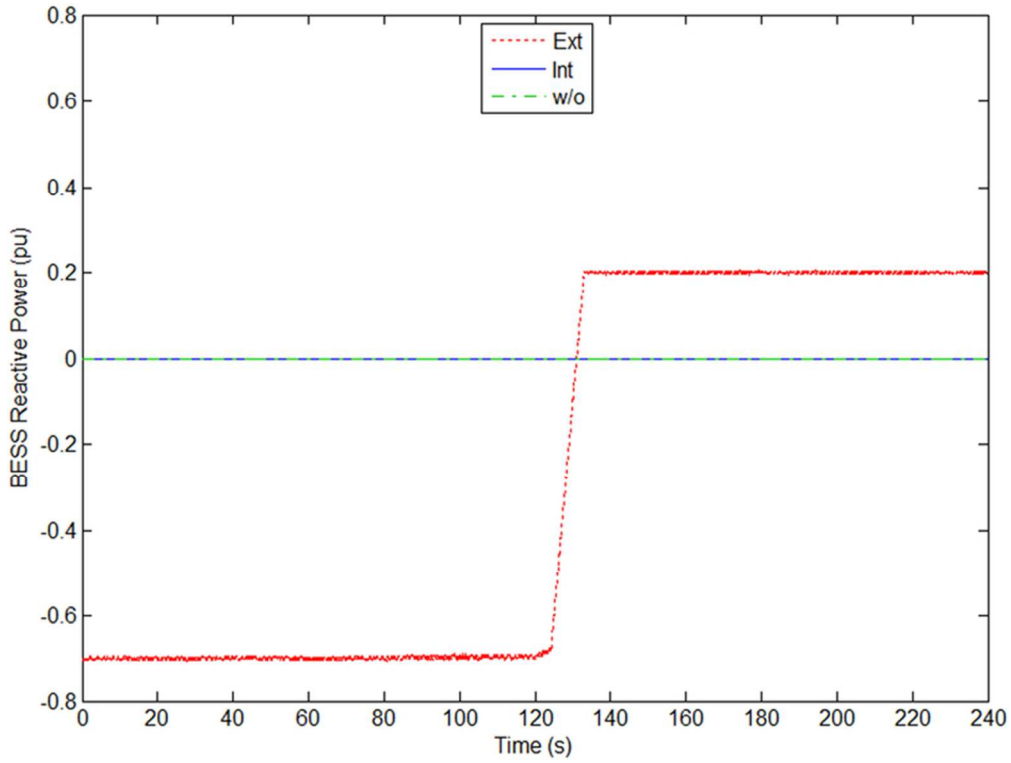

Figure 11
67x51mm (300 x 300 DPI)

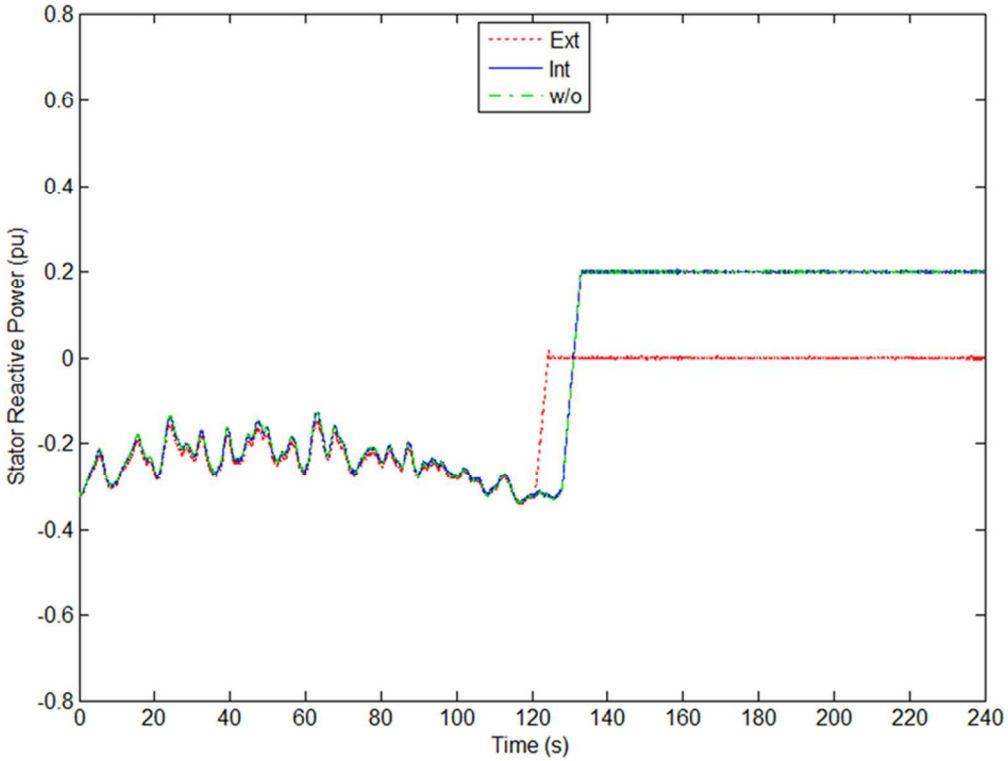

Figure 12
67x51mm (300 x 300 DPI)

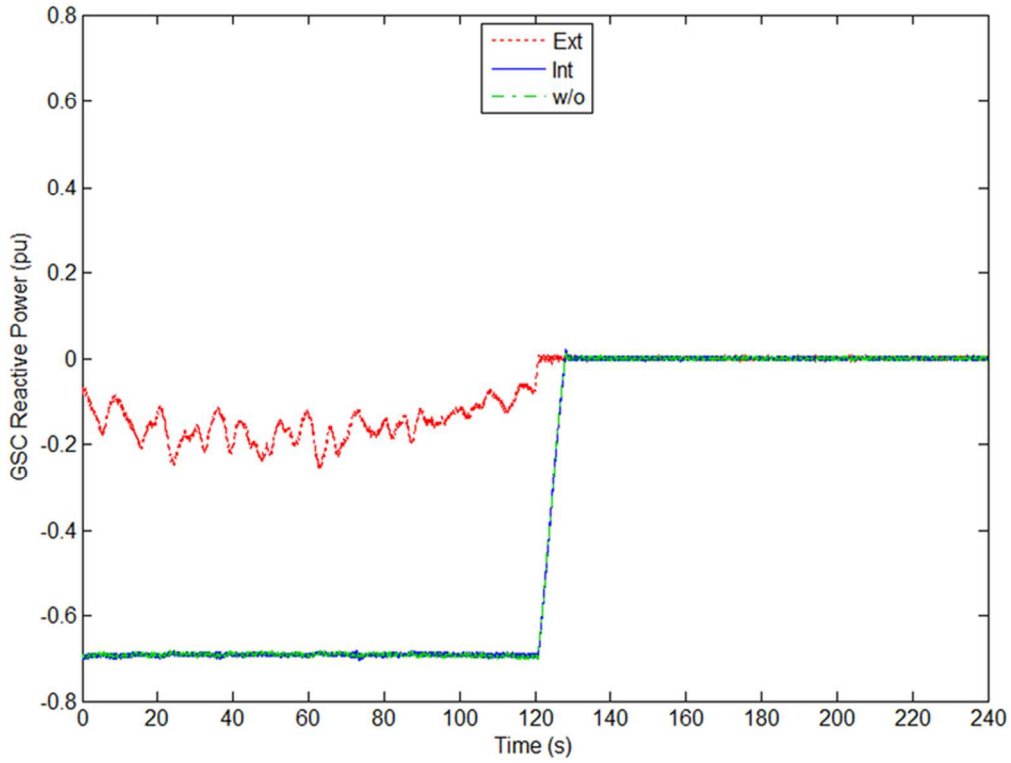

Figure 13
67x51mm (300 x 300 DPI)

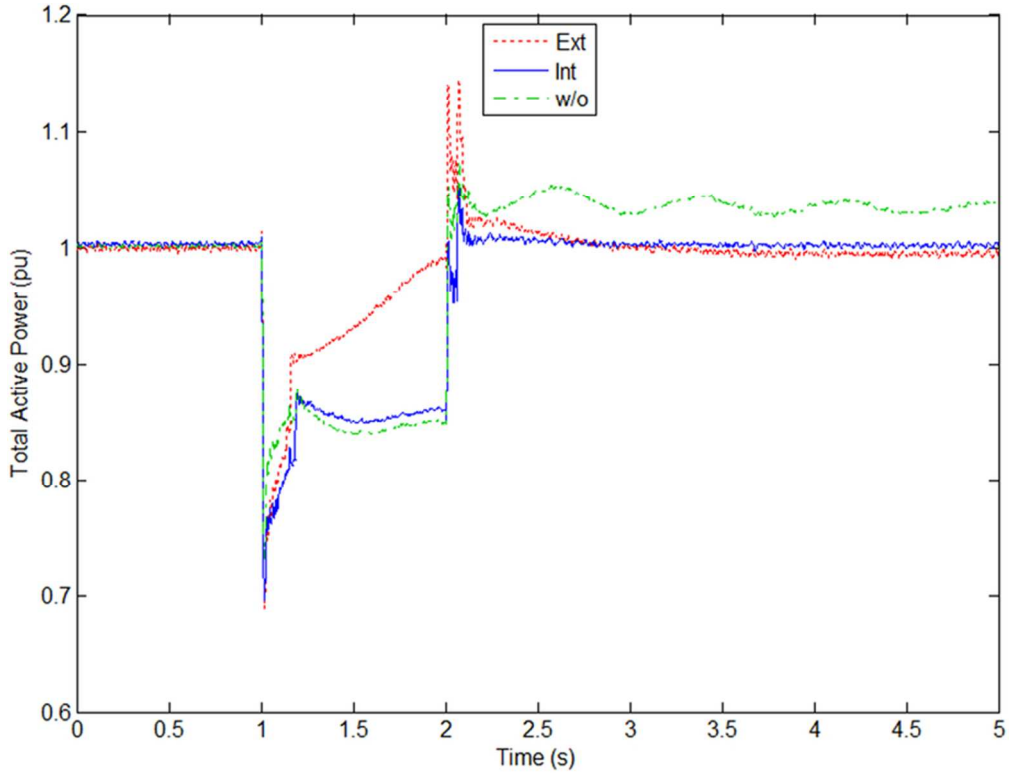

Figure 14
69x53mm (300 x 300 DPI)

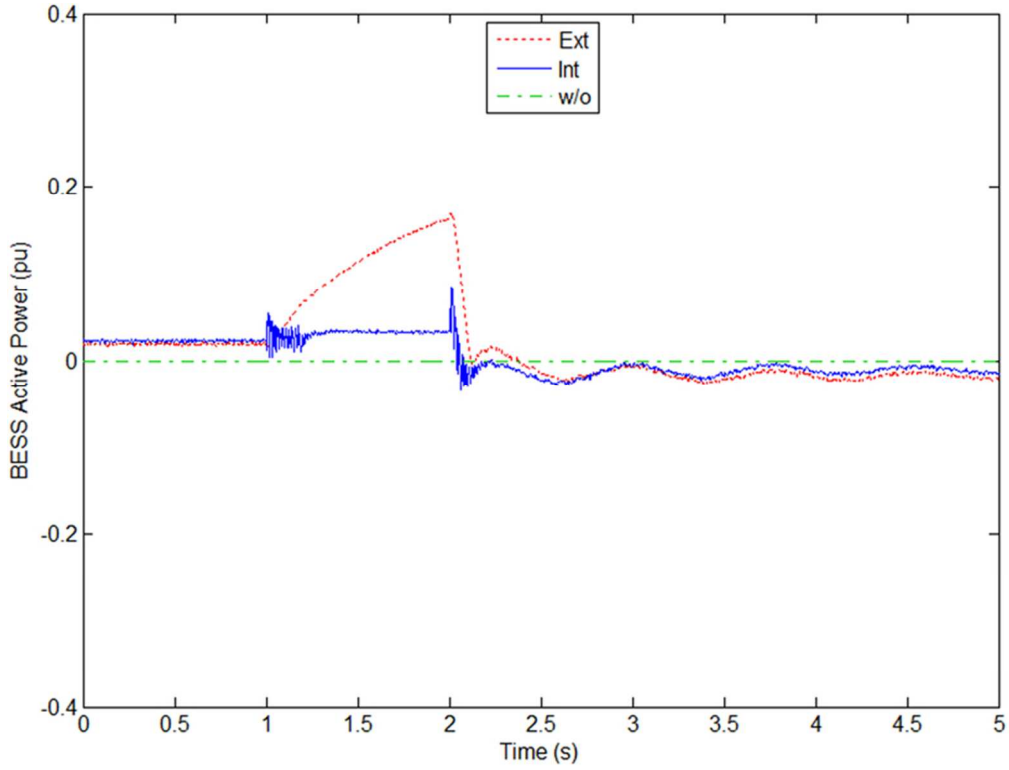

Figure 15
68x52mm (300 x 300 DPI)

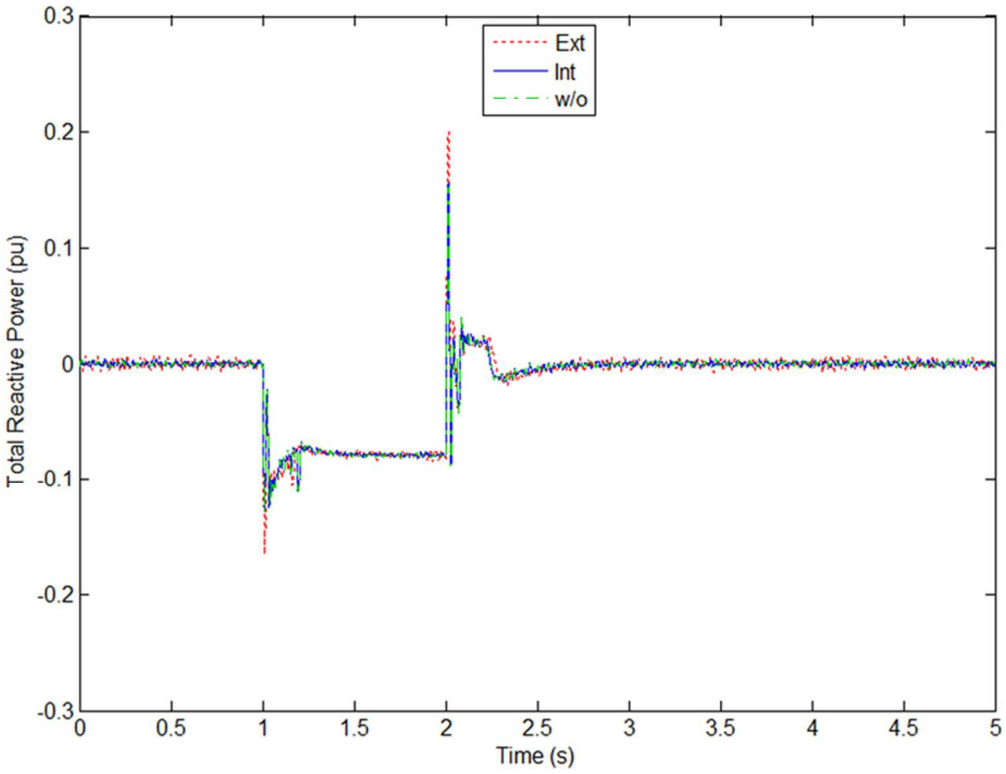

Figure 16
68x52mm (300 x 300 DPI)

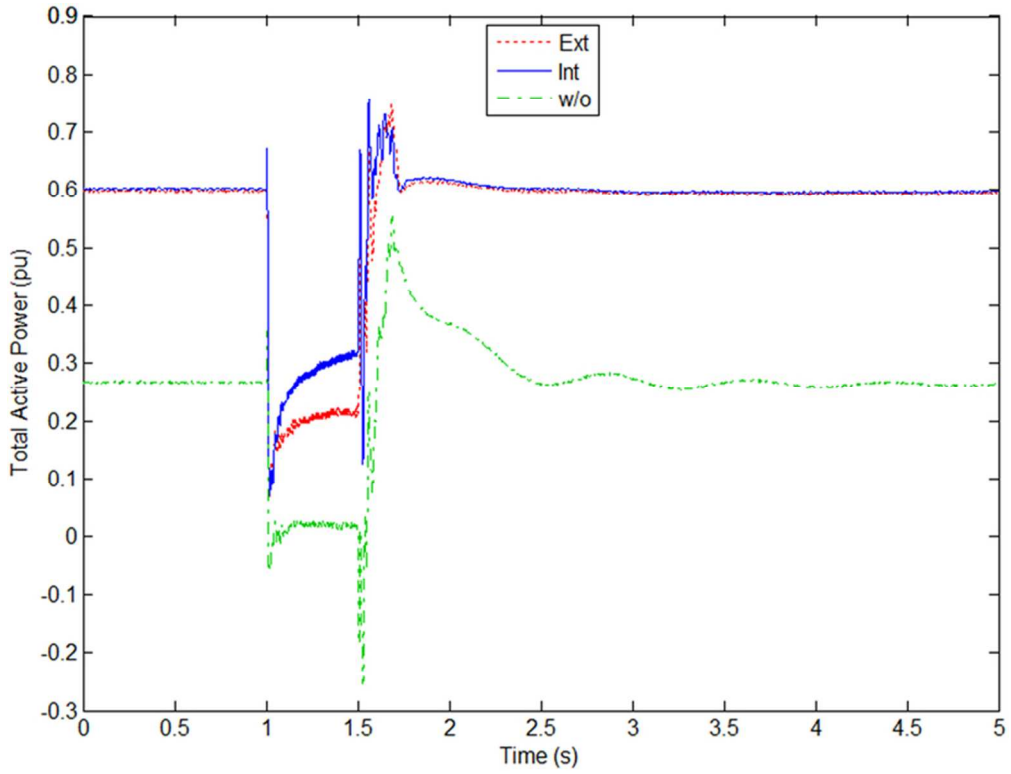

Figure 17
68x52mm (300 x 300 DPI)

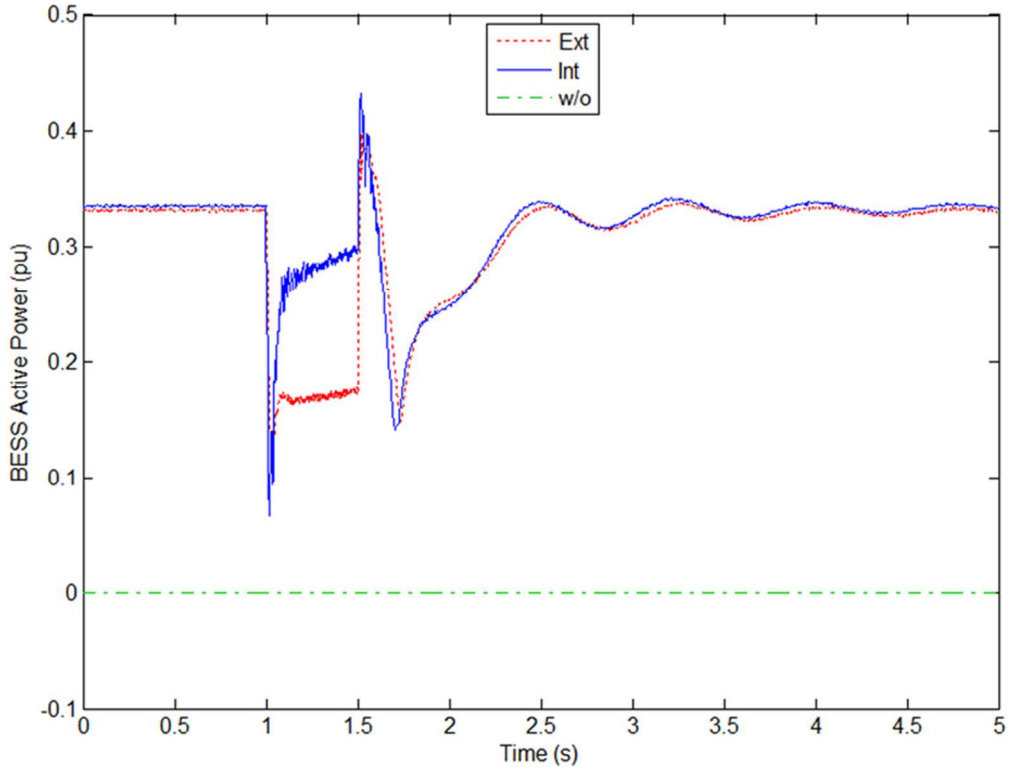

Figure 18
68x52mm (300 x 300 DPI)

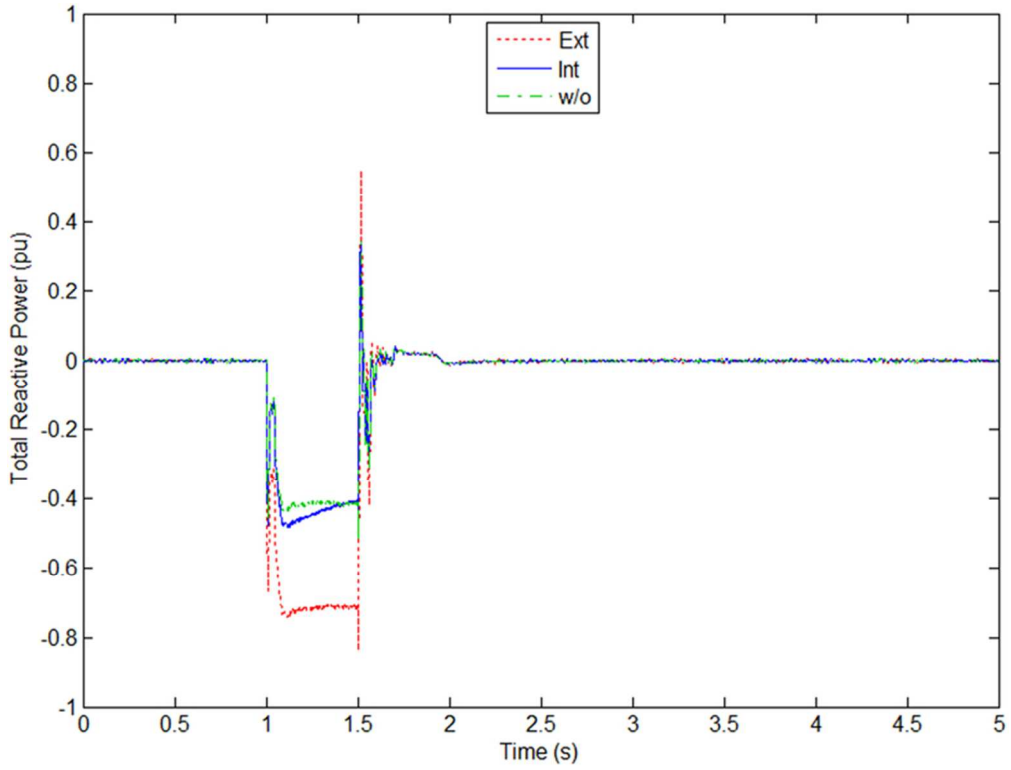

Figure 19
68x52mm (300 x 300 DPI)

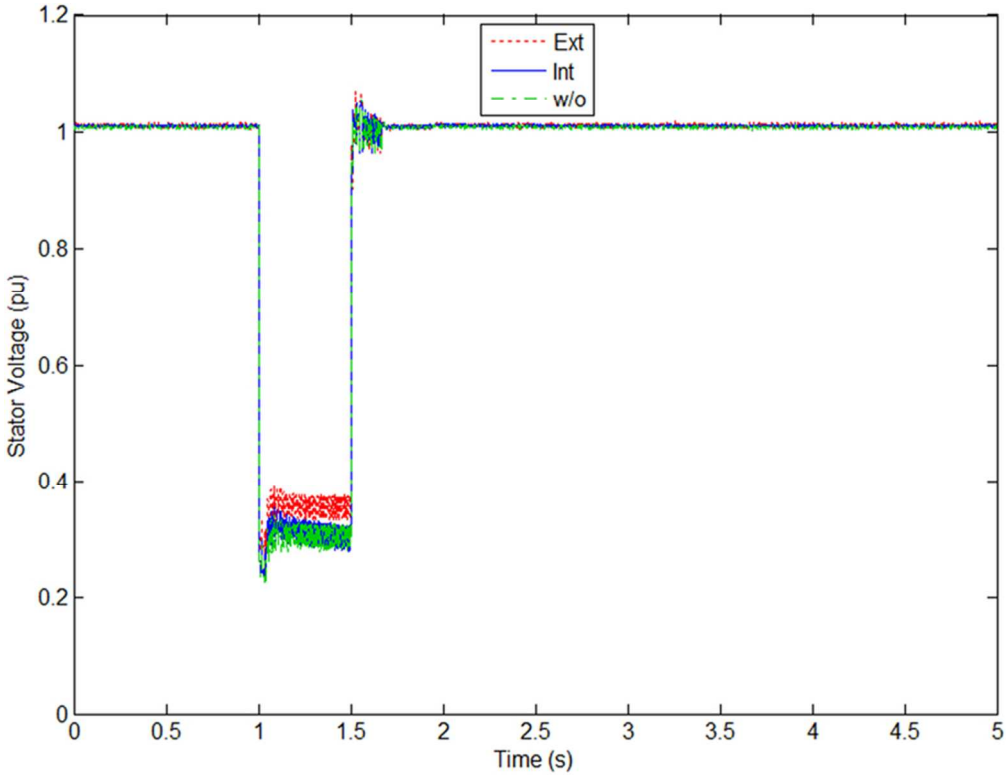

Figure 20
69x53mm (300 x 300 DPI)